Experimental study of Fe-Mn minerals as low-cost oxygen carriers in Chemical Looping Combustion Processes

ANTIGONI EVDOU[1,2], VASSILIS ZASPALIS[1,2], LORI NALBANDIAN[1]
Laboratory of Inorganic Materials, Chemical Process and Energy Resources Institute, Centre for Research and Technology-Hellas, 6th km, Harilaou-Thermi Rd, 57001 Thermi-Thessaloniki, Greece
Department of Chemical Engineering, Aristotle University of Thessaloniki, 54124 Thessaloniki, GREECE
antigoni@cperi.certh.gr, zaspalis@cperi.certh.gr, nalbanti@cperi.certh.gr

Abstract: - The main challenge in the technology of Chemical Looping Combustion (CLC) is to find viable candidate materials for use as "oxygen carriers". Low cost, naturally occurring minerals are examined in this work, which can substitute costly manufactured materials with comparable compositions. Two minerals with high content of Fe and Mn oxides are studied experimentally in the CLC process. Both materials exhibit satisfactory performance in terms of Oxygen Transfer Capacity (OTC), activity towards CH_4 oxidation, low selectivity to CO and H_2, and stability in multiple redox cycles. The materials are physicochemically characterized before and after their use, in order to investigate changes in their physicochemical properties as a result of multiple redox cycles.

Key-Words: - chemical looping combustion, CLC, low cost minerals, iron-manganese ore, oxygen carrier

1 Introduction

The combustion of fossil fuels is one of the major sources of carbon dioxide (CO_2) which is a greenhouse gas. Concern about the global climate change [1-4] prompted research on lowering CO_2 emissions during fossil fuel combustion. Commercial CO_2 capture technologies that exist today are expensive and energy intensive [5]. The main disadvantage of these techniques is the large amount of energy that is required for the separation, reducing the overall efficiency of a power plant.

Chemical looping combustion (CLC) has been suggested as an energy-efficient method for producing high purity CO_2 from combustion of fuel. Chemical-looping Combustion (CLC) is an in-situ CO_2 capture technology and offers a solution for CO_2 separation without energy penalty. The advantage with this technique as compared to conventional combustion is that CO_2 and H_2O are inherently separated from the other components of the flue gas, namely, N2 and unreacted O_2, and thus no extra energy is needed for CO_2 separation. It is a novel combustion technology [6] that involves the use of an oxygen carrier, such as a metal oxide, that transports oxygen from the air to the fuel, thereby avoiding direct contact between fuel and air.

The CLC system (Fig. 1) comprises two reactors, an air reactor and a fuel reactor. In the fuel reactor, the fuel reacts with the metal oxide. The reduced metal oxide is oxidized in the air reactor to form metal oxide. The regenerated metal oxide is ready to initiate a second cycle.

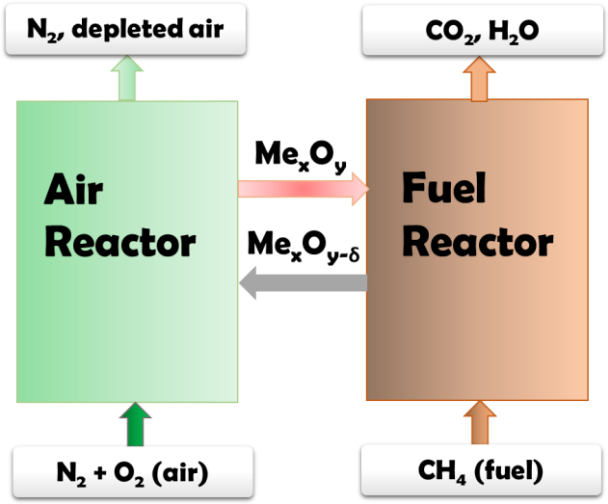

Fig. 1. Schematic of the Chemical looping combustion process

The exit stream from the fuel reactor contains only CO_2 and H_2O, thus after condensation of the H_2O, produces a pure CO_2 stream that can be directly sequestrated. The significant advantage of CLC compared to normal combustion is that a concentrated CO_2 stream, which is not diluted by N_2, can be obtained spending minimal energy for separation.

The main challenge in the technology of Chemical Looping Combustion is to find suitable materials for

use as "oxygen carriers". In order to be a viable candidate for the CLC process, the oxygen carrier material (OCM) must meet the following criteria [7]:

- sufficient oxygen transfer capacity
- satisfactory reactivity over the multiple cycles
- high mechanical integrity
- low tendency to agglomeration, fragmentation and attrition
- good resistance to sintering
- low possibility of deactivation by carbon deposition or sulphur compounds
- low cost
- environmental friendly

Experiments carried out using methane and syngas as fuel, show that Fe, Mn, Cu and Ni oxides are the most suitable, presenting the following relative reactivity $NiO > CuO > Mn_3O_4 > Fe_2O_3$ [9], [10]. However, nickel and copper oxides have a considerably higher cost. Conversely, materials containing Fe and Mn are attracting considerable interest, mainly because of their high availability and low cost [6]-[11].

It has been proven that pure iron oxide sources have to some extent difficulties to fully combust the fuel unless a high load of material is circulated. Another issue with these materials is related to the swelling of the material after several cycles, which is detrimental if long life-time is required [6]. On the other hand, manganese oxides are very promising oxygen carrier materials, given the fact that they can convert the fuel and give full combustion. However, attrition issues with such materials have often been observed.

As a means to enhance the mechanical strength of the particles, to be used in a circulating bed, a binder can be added to the redox active phase, however this would decrease the OTC and the activity of the Oxygen Carrier. Alternatively, one of the redox active phases could also act as an inherent support. It has been previously demonstrated that iron oxide can stabilize the performance of manganese oxides, thus mixed Fe-Mn oxides show great potentials as oxygen carrier materials for CLC [11]-[13].

Since CLC technology requires a significant amount of oxide carrier, the use of natural minerals would be advantageous. Raw minerals from different mining ores are natural choices for OCM since sufficient amounts are available within reasonable cost, even though such minerals might have high composition and quality variations [8]. In the present work the use of two minerals with high content of Fe and Mn oxides as oxygen carriers in Chemical Looping Combustion is explored. The performance of the candidate materials is ranked by taking into account their Oxygen Transfer Capacity (OTC), the methane conversion during the fuel oxidation step as well as the H_2 and CO selectivities, and their stability after repeated redox cycles.

2 Experimental Part

The minerals were selected based on their content in iron and manganese oxides, as well as trace elements content, their non-toxicity, low cost and availability. The following natural materials are tested in this study:

1. a Fe-Mn based mineral, from El-Waleed - Egypt named “Sinai-A, low grade”, with code name S12
2. a Fe-Mn based mineral, from El-Waleed - Egypt named “Sinai-A, medium grade”, with code name S22

Samples of both fresh materials and materials used in several redox cycles are physicochemically characterized by using the following methods:

- Elemental analysis by Inductively Coupled Plasma Optical Emission Spectroscopy (ICP-OES), using a Perkin Elmer, Optima 4300DV instrument,
- N_2 adsorption – desorption isotherms at the boiling point of liquid nitrogen (77 K) using a Micromeritics, Tristar instrument, to determine specific surface area, pore volume and pore size distribution,
- X-ray diffraction (XRD) for the identification of the crystalline phases formed in the prepared samples Powder XRD patterns are recorded with a Siemens D500 X-ray diffractometer,
- Morphological observation and elemental Microanalysis of the samples at a Scanning Electron Microscope (JEOL 6300) equipped with an X-ray EDS analyzer (Oxford Isis 2000).

The capability of the materials to deliver oxygen at high temperatures and convert CH_4 to synthesis gas during the fuel oxidation step, as well as their ability to reversibly pick up oxygen during the solid oxidation step is evaluated by pulse reaction experiments in a fixed bed pulse reactor. Reaction experiments with the materials in powder form are performed at 1273K, in a reaction unit (Altamira AMI-1) using a U-type quartz reactor into which 200±3 mg solid material is inserted. A detailed description of the experimental unit is provided elsewhere [14], [15]. During the fuel oxidation step, methane is fed to the reactor at constant volume pulses, through a special closed loop valve. Each pulse has of volume of 100μL. During the solid oxidation step, oxygen is injected to the reactor, also at constant volume pulses, at its entrance before the solid OC. The products at the output of the reactor are

continuously monitored by mass spectrometer (Balzers, Omnistar) and analyzed quantitatively, based on calibration curves for all reactants and products of the process.

3 Results – Discussion

The specific surface area of the materials, as received, without any pretreatment, as measured by N_2 sorption, is presented in Table 1.

Table 1: Surface area of materials

	S12	*S22*
Surface area (m^2/g)	27.61	20.83

In Table 2 the elemental composition, of the 2 materials is presented, as measured by ICP-OES in the form of oxides.

Table 2. Elemental composition of materials

	S12 (% wt)	*S22 (% wt)*
Fe_2O_3	60.05	32.71
MnO_2	23.26	39.06
SiO_2	10.94	21.40
CaO	1.31	2.47
Al_2O_3	1.92	1.28
BaO	0.92	1.44
MgO	0.61	0.61
Na_2O	0.32	0.28
ZnO	0.19	0.28
K_2O	0.22	0.18
TiO_2	0.10	0.10
Co_2O_3	0.01	0.01
NiO	0.02	0.02
V_2O_5	0.03	0.01
Cr_2O_3	0.000	0.01
CuO	0.03	0.08
PbO_2	0.03	0.03
AsO_2	0.01	0.01
Total	**100**	**100**

Both materials have high concentrations of Fe and Mn oxides. Si, Ca, Al and Ba oxides appear also at significant levels. S12 has the highest Fe content, while S22 has higher concentrations of Mn and Si oxides

The XRD patterns of the two mineral samples, as received, without any pretreatment are presented in Fig. 8 and Fig. 9, where also the crystalline phase identification for both materials is included. It is observed that for both materials the main phases are hematite (Fe_2O_3), tetravalent manganese oxide (MnO_2) and silica (SiO_2). The relative intensities of the peaks are in agreement with the concentration of each oxide, as measured by elemental analysis (Table 2).

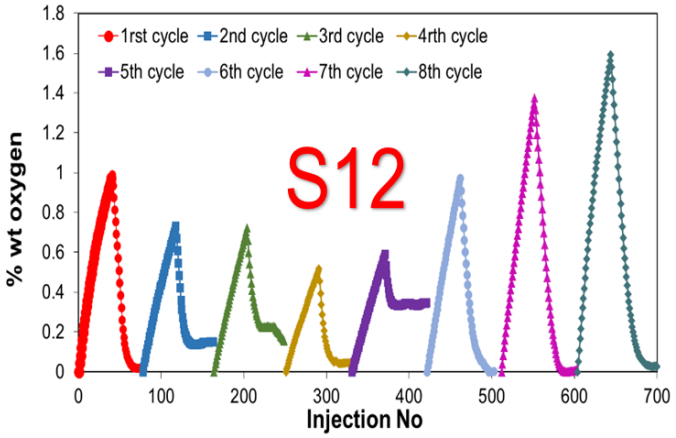

Fig. 2 Oxygen loss and uptake of sample "Sinai-A, low grade" (S12), during 8 subsequent reduction – oxidation cycles

In Fig. 2 the amount of oxygen exchanged by the mineral, "Sinai-A, low grade" (S12) is presented during an experiment which includes 8 multiple reduction – oxidation cycles. It can be observed that in the 1rst cycle an oxygen transfer capacity (OTC) of 1% wt is observed, the OTC is gradually decreasing during the first 4 cycles, however, it appears that the material is activated after cycle No 5, reaching an OTC of 1.6% in cycle No 8.

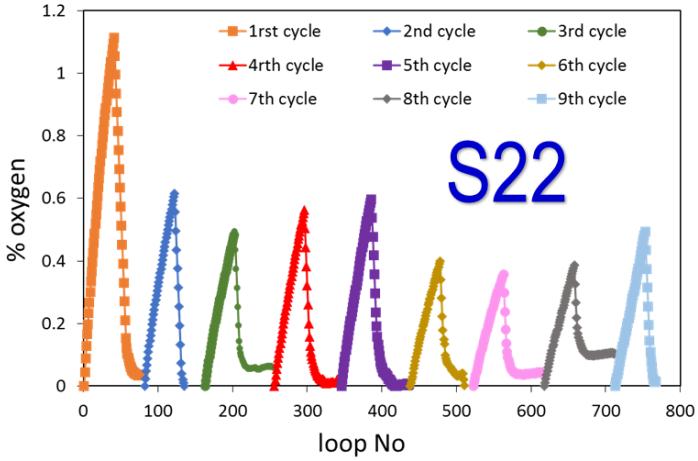

Fig. 3 Oxygen loss and uptake of sample "Sinai-A, medium grade" (S22), during 9 subsequent reduction – oxidation cycles

In Fig. 3 the amount of oxygen exchanged by the mineral, "Sinai-A, medium grade" (S22) is presented during an experiment which includes 9 multiple reduction – oxidation cycles. It can be observed that the oxygen transfer capacity (OTC) of the sample in the 1rst cycle is 1.1% wt, higher than the corresponding OTC of S12 material. However it is

gradually decreasing during subsequent cycles and is stabilized, during cycles 3-9, at 0.5±0.1% wt. The above results are summarized in Fig. 4.

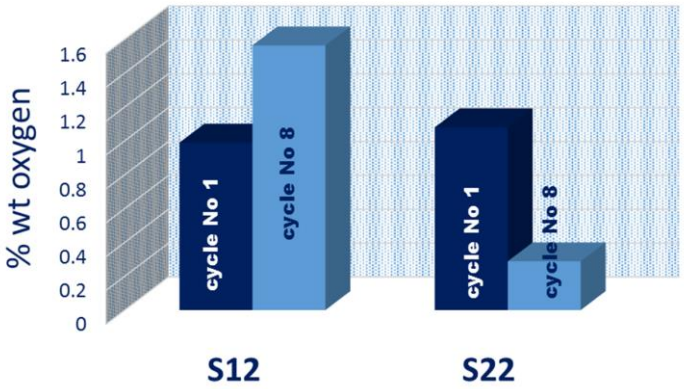

Fig. 4 Oxygen Transfer Capacity of the two minerals S12 and S22 during the 1rst and the 8th reduction – oxidation cycle.

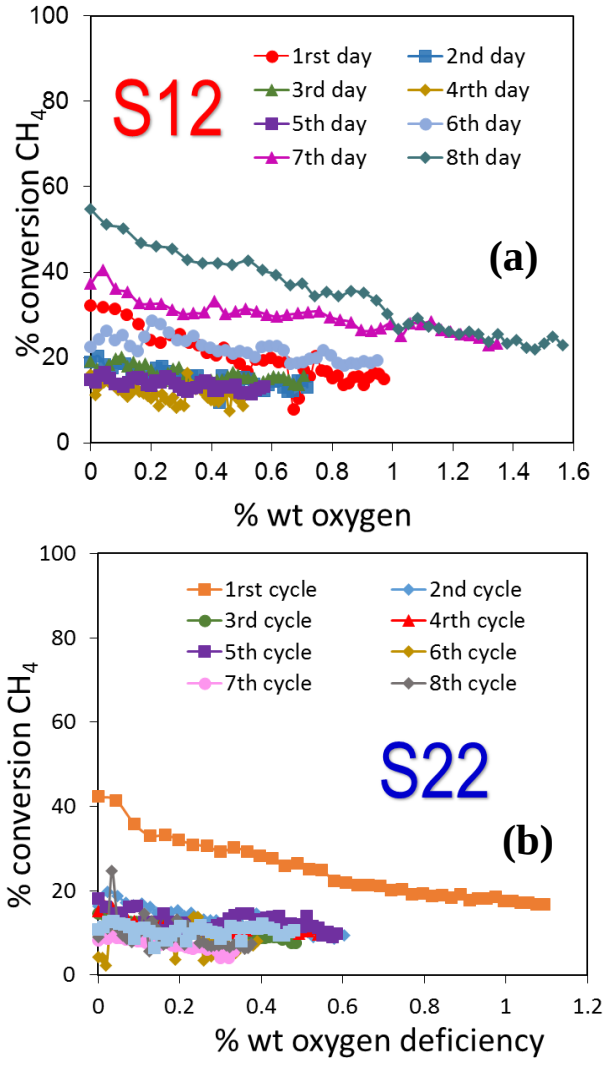

Fig. 5 Methane conversion by the (a) S12 sample and (b) S22 sample, vs. oxygen deficiency during multiple reduction – oxidation cycles

In Fig. 5a the reactivity of the natural material S12 is presented, expressed as % wt conversion of methane during the fuel oxidation step vs. oxygen deficiency during 8 subsequent reduction – oxidation cycles. The mineral has a moderate initial reactivity converting only ~40% at the 1rst cycle, when the material is fully oxidized. However, after the activation of the material beyond the 5th cycle, shown also in Fig. 2, its initial reactivity increases reaching initial methane conversion of ~55% at the 8th cycle. During all cycles, the initial reactivity of the fully oxidized material decreases with increasing oxygen deficiency, reaching a methane conversion of ~30% at the end of 8th cycle.

In Fig. 5b the reactivity of the natural material S22 is presented, expressed as % wt conversion of methane during the fuel oxidation step vs. oxygen deficiency during 9 multiple reduction – oxidation cycles. The initial conversion at the beginning of the 1st cycle, 40%, is not recovered from the material in the subsequent cycles.

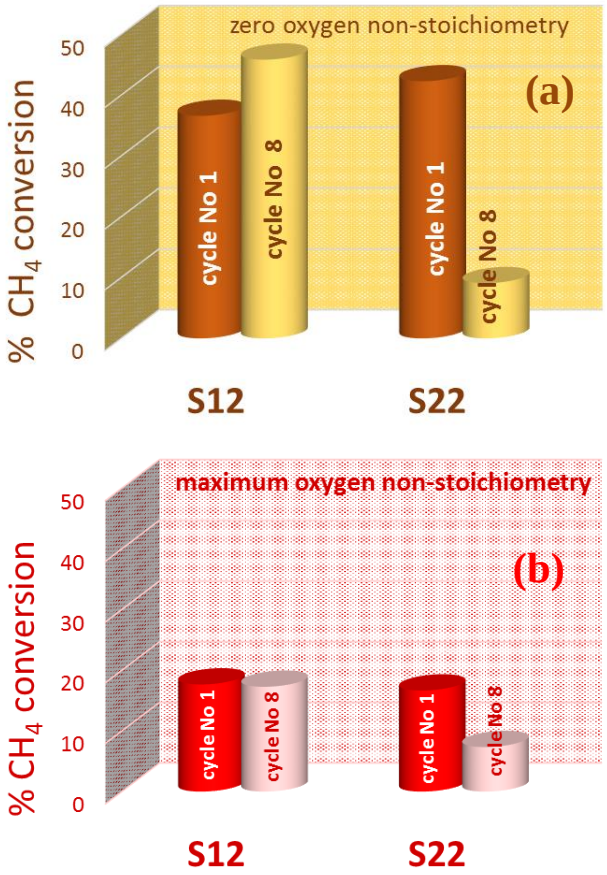

Fig. 6 CH_4 conversion at (a) "zero" and (b) "maximum" oxygen non – stoichiometry during the 1rst and the 8th reduction – oxidation cycle.

In Fig. 6 the above results are summarized and CH_4 conversion is compared at "zero" and "maximum" oxygen non – stoichiometry during the 1rst and the 8th redox cycle.

Since the materials are candidate Oxygen Carriers for Chemical Looping Combustion, they must have very low selectivity towards CO during fuel oxidation. In Fig. 7 the CO selectivity is presented for the two minerals S12 and S22 during the 1rst and the 8th reduction – oxidation cycle, and the values at "zero" and "maximum" oxygen non – stoichiometry are compared. It can be observed that CO selectivity increases with increasing oxygen deficiency of the solid and changes with increasing cycle number. In all cases, selectivity towards CO is always lower than 20%. It can be also observed that CO selectivity increases with decreasing reactivity of the material, which can be readily attributed to the decreased availability of lattice oxygen from the solid.

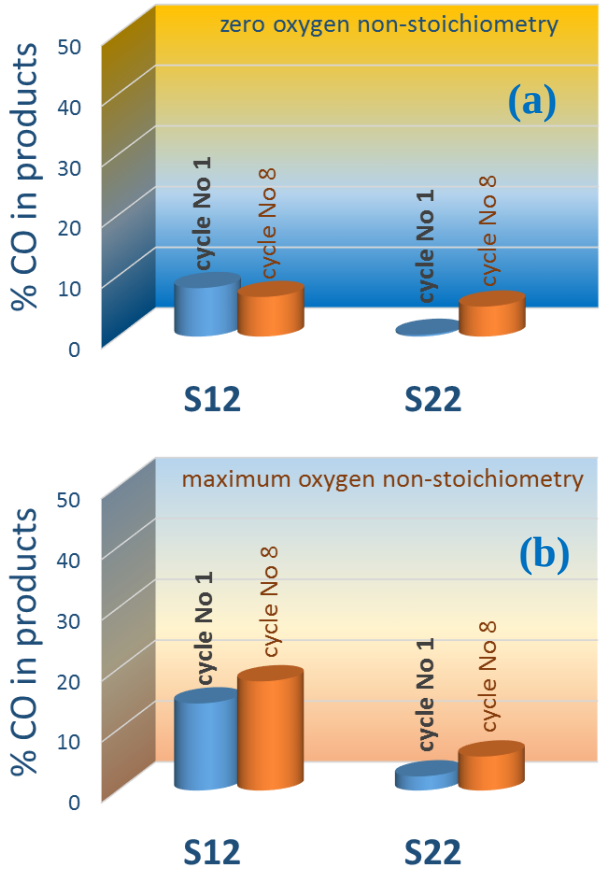

Fig. 7 Selectivity to CO at (a) "zero" and (b) "maximum" oxygen non – stoichiometry during the 1rst and the 8th reduction – oxidation cycle.

The XRD patterns of the S12 mineral sample, fresh and after 8 redox cycles are compared in Fig. 8.

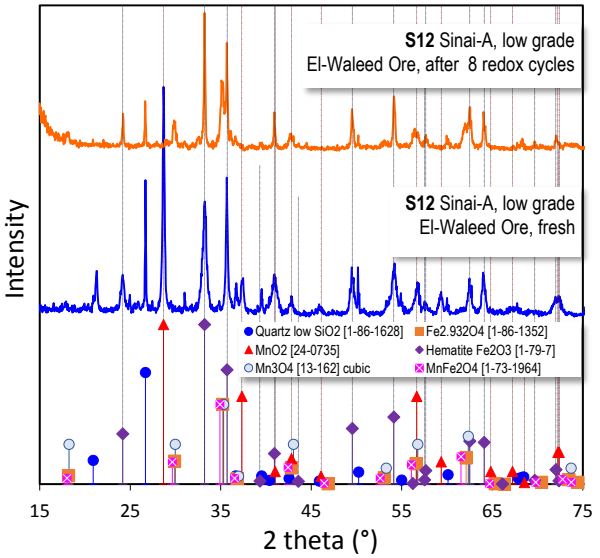

Fig. 8 X-ray diffraction (XRD) patterns of the S12 mineral sample, fresh and after 8 redox cycles

Identification of crystalline phases is also included in the Figure. In the fresh sample iron is trivalent, in the hematite (Fe_2O_3) phase and manganese is tetravalent, in the MnO_2 phase. It can be observed in the XRD pattern of the "reacted" sample that all peaks attributed to MnO_2 completely disappear, indicating that MnO_2 has decomposed. Also the peaks attributed to Fe_2O_3 are much less intense. New peaks arise in the XRD of the "used" sample which are attributed to spinel type oxides, either simple Fe_3O_4, Mn_3O_4, or mixed $MnFe_2O_4$.

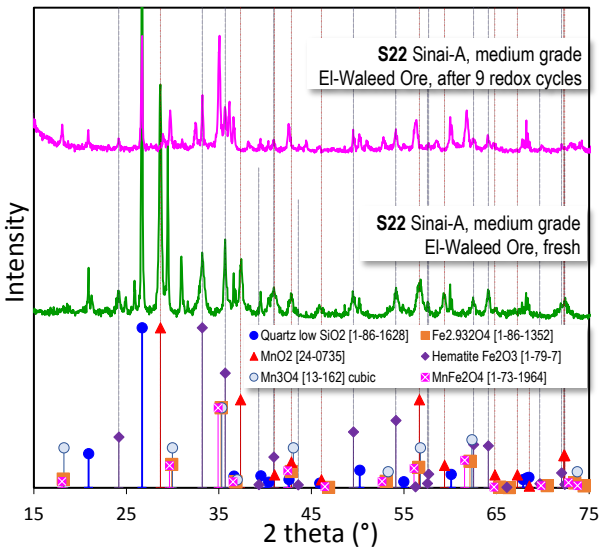

Fig. 9 X-ray diffraction (XRD) patterns of the S22 mineral sample, fresh and after 9 redox cycles

In Fig.9 the XRD patterns of the S22 mineral sample, fresh and after 9 redox cycles are compared. Despite the differences in the elemental composition of two minerals, the changes observed in the samples that have undergone multiple redox cycles are identical. Also in the S22 sample, the 4-valent manganese oxide disappears with simultaneous formation of a spinel phase, while part of hematite is also converted to magnetite.

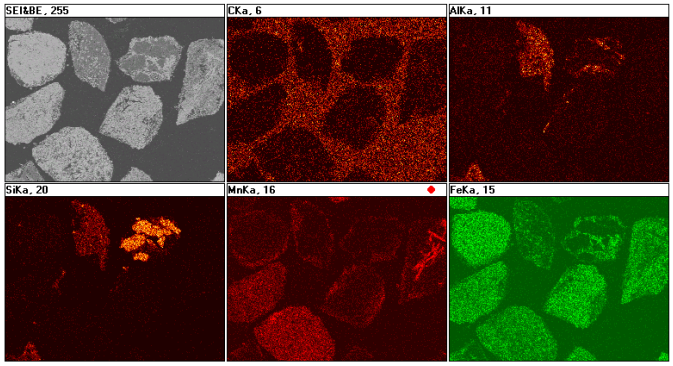

Fig. 10 Elemental mapping of particles of the "fresh" material S12, at low magnification (X200)

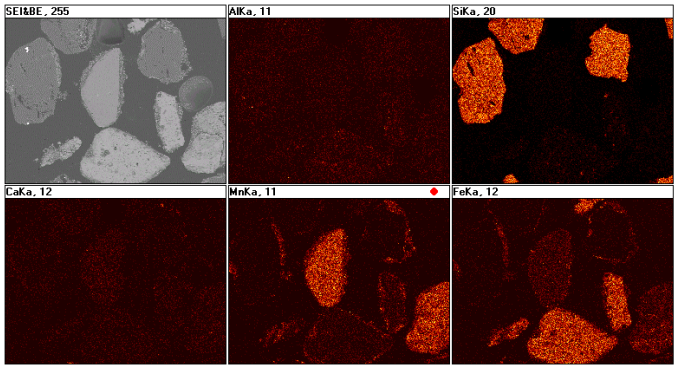

Fig. 11 Elemental mapping of particles of the fresh S22 mineral (magnification X200)

Both materials studied are natural minerals and show, as expected, great composition heterogeneity. Fig. 10 and Fig. 11 show the elemental mapping of grains from the "fresh" materials S12 and S22 respectively, at relatively low magnification (X200), to include a sufficient number of particles. It is observed that, for both materials, there are grains composed almost entirely of iron oxides, and other grains contain almost only Mn oxides. There are of course granules containing both elements. The maps of the lower concentrations elements, e.g. Si, Al, Ca, K, Mg show that they, also, are not evenly distributed. In the images of Fig. 8 either whole grains or large grain parts can be observed, with concentrations of these elements much higher than average.

In Fig. 12, Scanning Electron Microscopy (SEM) images are compared, of the S12 mineral, fresh and after 8 redox cycles, at the same magnification level.

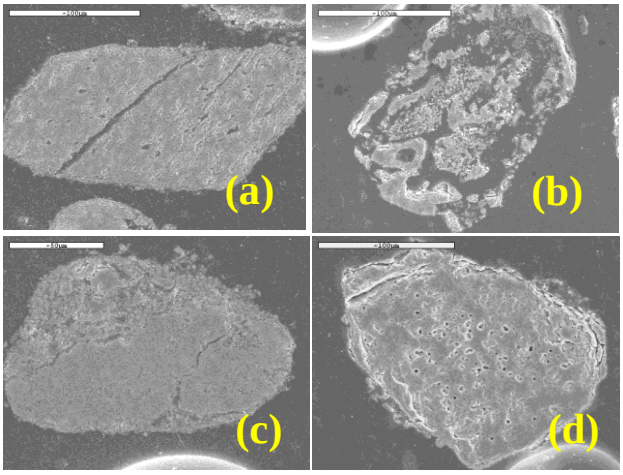

Fig. 12 Scanning Electron Microscopy (SEM) images of the S12 mineral. (a) fresh Mn-rich particle (b) Mn-rich particle after 8 redox cycles (c) fresh Fe-rich particle (d) Fe-rich particle after 8 redox cycles

The particles Fig. 12a and 12b are rich in Mn while those in the Fig. 12c and 12d are composed almost 100% by Fe-oxides. A completely different effect in the morphology of the particles can be observed, of subjecting the material to multiple redox cycles, depending on their chemical composition. While the Mn-rich particles undergo extensive erosion, the Fe-rich particles remain almost unaffected. It is observed that the extent of disintegration is a function of the duration, the intensity and the number of redox cycles that the material suffered.

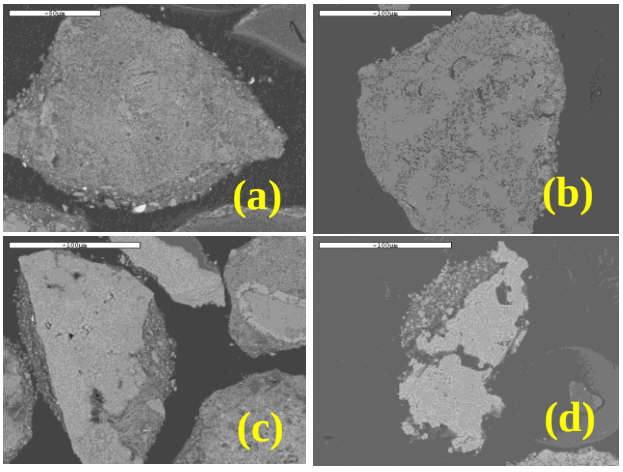

Fig. 13 Scanning Electron Microscopy (SEM) images of the S22 mineral. (a) fresh Mn-rich particle (b) Mn-rich particle after 8 redox cycles (c) fresh Fe-rich particle (d) Fe-rich particle after 8 redox cycles

The same changes are observed also in the case of S22 particles, as shown in the SEM images of Figure 13.

4 Conclusion

The two examined natural materials have the ability

to deliver lattice oxygen to a fuel and to regain it in the presence of air. The S12 material, with a high content of Fe oxides (60%) and ratio Fe/Mn≈2.5 shows higher values than the S22 material, with lower level of Fe oxide (33%) and ratio Fe/Mn≈1, as regards both the Oxygen Transfer Capacity (OTC) and the activity towards CH_4 conversion

The S12 material is further activated after 4 oxidation - reduction cycles. Both materials lead to complete combustion of methane, with selectivities towards CO and H_2 lower than 10%. Therefore both minerals are promising candidate materials for use as "oxygen carriers" in the chemical looping combustion process (CLC) with the best performance shown by the S12, which is considered a low grade mineral.

Physicochemical characterization of samples of the natural materials, fresh – unreacted and "reacted" at subsequent redox cycles, revealed that repetitive reduction–oxidation reactions affect seriously both the crystalline structure of the materials and their particle morphology. Most of the Mn and Fe oxides are converted into magnetic cubic spinels in the "reacted" samples. Furthermore multiple redox cycles at high temperature, cause erosion to the Mn particles, which leads to extensive breaking of the large particles and the formation of smaller particles, while the particles which are rich in Fe do not undergo any change in their morphology.

References:

[1] J.C.M.Pires, F.G. Martins, M.C.M. Alvim-Ferraz, M. Simões, "Recent developments on carbon capture and storage: An overview" *Chemical Engineering Research and Design*, vol. 89, 2011, pp. 1446-1460

[2] N. Pessel, J.F. Balmat, "Principal Component Analysis for Greenhouse Modelling", *WSEAS Transactions on Systems*, Vol. 7, 2008, pp. 24-30

[3] M. Lanfranchi, C. Giannetto, A. De Pascale, "Economic Implications of Climate Change for Agricultural Productivity", *WSEAS Transactions on Environment and Development*, Vol. 10, 2014, pp. 233-241

[4] Mirela Matei, Cătălin Popescu, Irina Gabriela Rădulescu, "The Consequences of Climate Change and Social Responsible Behaviour", *WSEAS Transactions on Business and Economics*, Vol. 9, 2012, pp. 29-38

[5] Julija Gusca, Irina Naroznova, Dagnija Blumberga, Anna Volkova, "Carbon capture and storage: cost analysis of electricity production for Latvia", *International Journal of Energy*, Vol. 4, 2010, pp. 37-45

[6] J. Adanez, A. Abad, F. Garcia-Labiano, P. Gayan, L.F. de Diego, "Progress in chemical-looping combustion and reforming technologies," *Progress in Energy and Combustion Science*, vol. 38, 2012, pp. 215-282.

[7] M. Johansson, T. Mattisson, A. Lyngfelt, "Comparison of oxygen carriers for chemical-looping combustion," *Thermal Science*, vol. 10, 2006, pp. 93-107.

[8] A. Fossdal, E. Bakken, B.A. Øye, C. Schøning, I. Kaus, T. Mokkelbost, Y. Larring, "Study of inexpensive oxygen carriers for chemical looping combustion," *International Journal of Greenhouse Gas Control*, vol. 5, 2011, pp. 483-488.

[9] M. Johansson, PhD Thesis, Chalmers University of Technology, Göteborg, Sweden, 2007.

[10] A. Abad, J. Adánez, F. García-Labiano, L. F. de Diego, P. Gayán, J. Celaya, "Mapping of the range of operational conditions for Cu-, Fe-, and Ni-based oxygen carriers in chemical-looping combustion," *Chemical Engineering Science*, vol. 62, 2007, pp. 533-549.

[11] A. Lambert, C. Delquié, I. Clémeneçon, E. Comte, V. Lefebvre, J. Rousseau, B. Durand, "Synthesis and characterization of bimetallic Fe/Mn oxides for chemical looping combustion," *Energy Procedia*, vol. 1, 2009, pp. 375-381.

[12] G. Azimi, H. Leion, T. Mattisson, M. Ryden, F. Snijkers, A. Lyngfelt, "Mn-Fe oxides with support of $MgAl_2O_4$, CeO_2, ZrO_2 and Y_2O_3-ZrO_2 for chemical-looping combustion and chemical-looping with oxygen uncoupling" *Industrial & Engineering Chemistry Research*, vol. 53, 2014, pp. 10358-10365.

[13] E. Ksepko, R. V. Siriwardane, H. Tian, T. Simonyi, M. Sciazko, "Effect of H_2S on chemical looping combustion of coal-derived synthesis gas over Fe-Mn oxides supported on sepiolite, ZrO_2, and Al_2O_3," *Energy & Fuels*, vol. 26, 2012, pp. 2461-2472.

[14] A. Evdou, V. Zaspalis, L. Nalbandian, "$La_{1-x}Sr_xFeO_{3-\delta}$ perovskites as redox materials for application in a membrane reactor for simultaneous production of pure hydrogen and synthesis gas," *Fuel*, vol. 89, 2010, pp. 1265-1273.

[15] L. Nalbandian, A. Evdou, V. Zaspalis, "$La_{1-x}Sr_xM_yFe_{1-y}O_{3-\delta}$ perovskites as oxygen-carrier materials for chemical-looping reforming," *Journal of Hydrogen Energy*, vol. 36, 2011, pp. 6657-6670.